INDERSCIENCE PUBLISHERS
Linking academia, business and industry through research

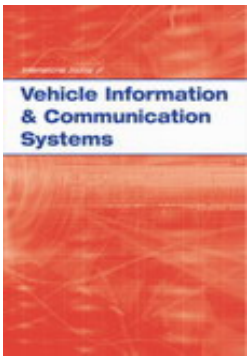

International Journal of Vehicle Information and Communication Systems

ISSN online: 1741-8208 - ISSN print: 1471-0242
https://www.inderscience.com/ijvics

Multi-user non-orthogonal waveform transceiver in RIS-assisted UAV communication: design and implementation

Md. Omor Faruk, Saifur Rahman Sabuj, S.K. Tamanna Kamal, Fowzia Jabin, Joarder Jafor Sadique, Shaikh Enayet Ullah

DOI: 10.1504/IJVICS.2025.10068810

Article History:

Received:	14 November 2023
Last revised:	30 May 2024
Accepted:	15 August 2024
Published online:	27 January 2025

Multi-user non-orthogonal waveform transceiver in RIS-assisted UAV communication: design and implementation

Md. Omor Faruk

Department of Electrical and Electronic Engineering,
University of Rajshahi,
Rajshahi, Bangladesh
Email: omor.apee.ru2011@gmail.com

Saifur Rahman Sabuj*

Department of Electrical and Electronic Engineering,
Brac University,
Dhaka, Bangladesh
Email: s.r.sabuj@ieee.org
*Corresponding author

S.K. Tamanna Kamal and
Fowzia Jabin

Department of Electrical and Electronic Engineering,
University of Rajshahi,
Rajshahi, Bangladesh
Email: tamanna.eee.ru@gmail.com
Email: fowziajabin.eeeru@gmail.com

Joarder Jafor Sadique

Department of Electrical and Electronic Engineering,
Begum Rokeya University,
Rangpur, Bangladesh
Email: joarder@brur.ac.bd

Shaikh Enayet Ullah

Department of Electrical and Electronic Engineering,
University of Rajshahi,
Rajshahi, Bangladesh
Email: enayet_apee@ru.ac.bd

Abstract: Reconfigurable Intelligent Surface (RIS) has evolved as an energy-efficient wireless communication technology and its anticipation with Unmanned Aerial Vehicles (UAV) has extended the millimetre wave range communications by enhancing wireless coverage. In this research article, we propose a downlink multi-user RIS-assisted Non-Orthogonal Waveform (NOW) transceiver system that is energy-efficient. A NOW approach for increasing spectrum efficiency through the integration of Faster-Than-Nyquist (FTN) signalling in DFT-s-OFDM is provided. In addition, we have implemented QR-GSO pre-coding algorithm for reducing Multi-User Interference (MUI). The simulated system incorporates Low-Density Parity Check (LDPC) and Repeats and Accumulates (RA) channel coding schemes along with various types of signal detection techniques such as Zero Forcing (ZF), Cholesky Decomposition (CD)-based ZF, Lattice Reduction-based MMSE (LR-MMSE) and Minimum Mean Square Error (MMSE) to improve Bit Error Rate (BER). Results from simulations demonstrate that the suggested system is effective with regard to of BER, energy efficiency and attainable spectral efficiency. The ground users achieve an improved BER performance with a value of 1×10^{-4} at 10 dB signal-to-noise ratio under RA with CD based ZF, 8 dB under RA with CD-based ZF, 10 dB under RA with LR-MMSE and 12 dB under RA with ZF.

Keywords: energy efficiency; faster-than-Nyquist signalling; millimetre-wave; non-orthogonal waveform; QR-GSO pre-coding; reconfigurable intelligent surfaces; unmanned aerial vehicle.

Reference to this paper should be made as follows: Faruk, M.O., Sabuj, S.R., Kamal, S.K.T., Jabin, F., Sadique, J.J. and Ullah, S.E. (2025) 'Multi-user non-orthogonal waveform transceiver in RIS-assisted UAV communication: design and implementation', *Int. J. Vehicle Information and Communication Systems*, Vol. 10, No. 1, pp.85–111.

Biographical notes: Md. Omor Faruk received his BSc Engineering and Master of Engineering Degrees in Applied Physics and Electronic Engineering (Presently renamed as Electrical and Electronic Engineering) from the University of Rajshahi, Rajshahi, Bangladesh, in 2015 and 2017, respectively. He worked as an Analyst at Kazi It Center Ltd, Rajshahi, Bangladesh, from 2017 to 2019. His major research interests include Machine Learning, Reinforcement Learning, Robotics, Wireless Communication System, 6G compatible terahertz IRS-NOMA, 5G compatible mmWave communications.

Saifur Rahman Sabuj is currently working with Electrical and Electronic Engineering Department as an Associate Professor at Brac University, Bangladesh. From 2020 to 2022, he worked as a Postdoctoral Research Fellow in the Electronic Engineering Department at Hanbat National University, South Korea. From 2008 to 2013, he was a faculty member of Green University of Bangladesh, Metropolitan University, Sylhet, and Bangladesh University. He received a Ph.D. degree in the Graduate School of Engineering, Kochi University of Technology, Japan in 2017. His research interests include MIMO-OFDM/NOMA, Cognitive Radio, Internet-of-things, Relay Networks, Unmanned Aerial Vehicle, and Machine-to-machine for wireless communications.

S.K. Tamanna Kamal is an accomplished individual who completed her Bachelor of Science in Electrical and Electronic Engineering (EEE) from the University of Rajshahi in 2022. Her interest in the field led her to pursue various research projects focused on nonorthogonal multiple access (NOMA), 6G compatible terahertz IRS-NOMA, 5G compatible mmWave

communications, massive MIMO, OFDM, GFDM, and physical layer security. Her exceptional academic performance and dedication to her field earned her the respect of her peers and professors. Currently, she is pursuing admission to a Master's degree programme to further deepen her knowledge and expertise in her research areas.

Fowzia Jabin is an accomplished individual who has completed her Bachelor of Science in Electrical and Electronic Engineering (EEE) from the University of Rajshahi in 2022. Currently, she is pursuing admission to a Master's degree programme to further deepen her knowledge and expertise in her research areas. Her interest in the field led her to pursue various research projects focused on non-orthogonal multiple access (NOMA), 6G compatible terahertz IRS-NOMA, 5G compatible mmWave communications, massive MIMO, OFDM, GFDM, and physical layer security. Her primary research interests include 5G/6G compatible mmWave hybrid precoded communications.

Joarder Jafor Sadique received his B.Sc. (Hons.) and M.Sc. degree in applied physics and electronic engineering (presently named as, electrical and electronic engineering) from University of Rajshahi, Rajshahi, Bangladesh in 2010 and 2011, respectively. He has been serving as an Assistant Professor with the electrical and electronic engineering department, Begum Rokeya University, Rangpur (BRUR), Bangladesh, since October 2017. He was also a faculty member of electrical and electronic engineering department at University of Information Technology and Sciences (UITS), Dhaka-1212, Bangladesh from May 2013 to March 2014. His main research interests include machine learning-based integrated terrestrial and non-terrestrial communication, unmanned aerial vehicle (UAV) mounted 5G and beyond millimetre wave communications, and intelligent reflecting surface (IRS)-assisted wireless networks.

Shaikh Enayet Ullah received B.Sc. (Hons.) and M.Sc. degrees in Applied Physics and Electronics from the University of Rajshahi, Rajshahi, Bangladesh, in 1981 and 1982, respectively, and a PhD degree from Jahangirnagar University, Dhaka, Bangladesh, in 2000. He has been working as a full professor in the Department of Applied Physics and Electronic Engineering (currently named Electrical and Electronic Engineering) at the University of Rajshahi from 2004 to 2024. He was the head of the Department of Information and Communication Engineering at the University of Rajshahi from January 2009 to January 2012. He was also the head of the Department from October 2013 to February 2015. His current research interests include B5G/6G compatible terrestrial and non-terrestrial (UAV-assisted) single/ multiple RIS-assisted mmWave/THz communications, interleave frequency division multiplexing (IFDM), delay-Doppler domain OFDM (DD-OFDM), orthogonal time sequencey multiplexing (OTSM), orthogonal chirp division multiplexing (OCDM), sparse code multiple access (SCMA), orthogonal time frequency space (OTFS), massive MIMO communications, fading and interference mitigation, channel equalization, and channel coding.

1 Introduction

As part of the third Generation of the Partnership Project (3GPP), commercial Fifth-Generation-New Radio (5G-NR) networks supporting the Internet of Things (IoT), multimedia-broadcast single frequency network (MBSFN) with NR-OFDM numerology and Enhanced Mobile Broadband (eMBB) have been implemented. The 5G NR networks use both millimetre wave (mmWave) and centimetre wave (cmWave) radio frequencies. For both downlink and uplink transmission in the 5G NR physical layer, Cyclic Prefix (CP)-based Orthogonal Frequency Division Multiplexing (OFDM) is used as the multiple access scheme, while CP-supportive Discrete Fourier Transform-spread-OFDM (DFT-s-OFDM) is used for single carrier frequency division multiple access (Zaidi et al., 2018; ETSI, 2018). Currently, 5G networks are confronted with unprecedented demand for high-quality and seamless wireless services for eMBB, massive Machine-Type Communications (mMTC) and Ultra-Reliable and Low-Latency Communications (URLLC). In 2030, beyond 5G (B5G) networks will not be able to satisfy all the needs of future cellular systems due to the revolutionary changes in individual and social trends brought on by the quick spread of entirely new IoT applications and visible improvement in human-machine interface technologies.

Keeping in mind the limitations of 5G networks, researchers from academia and industry have concentrated on sixth-generation (6G) wireless communication networks, which are anticipated to be capable of releasing the full potential of plentiful autonomous services containing both previous and future trends. The 6G wireless communication networks are anticipated to offer much greater energy/spectral/cost efficiency, 10 times lower latency, a higher data rate, more intelligence for full automation, sub-centimetre geolocation accuracy, 100 times higher connection density and close to 100% coverage. Owing to its enormous bandwidth, low latency, high rate and user-friendly locating function, mmWave communication with a frequency spectrum of 30 to 300 GHz will become one of the primary supporting technologies in 6G wireless communication systems. It is envisioned that Reconfigurable Intelligent Surface (RIS) will be used in 6G networks to increase the spectral efficiency, security, energy efficiency and communication dependability of 6G wireless networks (Xie et al., 2021; Zhang et al., 2021a).

1.1 Prior works

To give a substantial advantage to new communication technologies, researchers are prioritising the design of Reconfigurable Intelligent Surfaces (RIS) while taking into account issues such as Line-of-Sight (LOS) requirements and high path loss, as well as their usability in 6G networks. Chen et al. (2022) emphasised the developing RIS as a viable technique for improving the propagation environment and spectrum efficiency of wireless communications by managing low-cost passive reflecting parts. In their research, they had a constructive conversation about RIS-assisted channel estimation challenges in B5G/6G communications, such as Channel State Information (CSI) collection, imperfect cascade CSI for beamforming design and co-channel interference coordination. The authors developed a few prospective solutions or futuristic technologies to promote the development of B5G/6G in their work. The Ultra-Massive Multiple-Input Multiple-Output (UM-MIMO), RIS, cell-free massive MIMO and terahertz communications are among the primary prospective technologies for 6G mobile

networks that the authors of Cui et al. (2022) noted as sharing an exceptionally large-scale antenna array. They studied the upcoming near-field communication approaches for 6G in-depth and provided the principles of near-field communications as well as the metric for determining near-field ranges in common communication situations. The consequences of applying cutting-edge AI architectures, designs and techniques to various UAV-assisted Internet of Things (IoT) network aspects, such as important IoT technologies, duties and applications, was examined by the authors in Cheng et al. (2023). They also discussed possible areas of study and challenges for AI-enabled UAV-assisted IoT systems.

Liu et al. (2020) emphasised the use of a Non-Orthogonal Waveform (NOW) for 6G networks and demonstrated its superior spectral efficiency compared to discrete Fourier transform spreading OFDM (DFT-s-OFDM) waveform. The authors stated in Zhang et al. (2021b) that the inherent integration of Non-Orthogonal Multiple Access (NOMA) and RIS methods was envisioned as a potential way to greatly improving both spectrum efficiency and energy efficiency for future wireless communication networks. They investigated Physical Layer Security (PLS) for RIS-aided NOMA 6G networks in terms of both external and internal eavesdropping and required that the offered systems perform better. Hassouna et al. (2022) developed a wideband OFDM communication system based on a feasible RIS configuration with variable phase shifts for each element in the surface. In their simulation analysis, they found that applying high resolution discrete phase changes per RIS element resulted in a higher data rate. The authors of presented an innovative RIS Grouping-Based Index Modulation (RGB-IM) to increase spectral efficiency and Bit Error Rate in (BER) (Asmoro and Shin, 2022). In their study, they simulated and evaluated the proposed system's spectrum efficiency and BER using theoretical calculations, and the computer simulation results showed that the RGB-IM outperformed a relay-assisted spatial modulation. Because of the cost efficiency and installation flexibility, Sadique et al. (2022) emphasised a UAV communication system. In their research, they presented a cumulative effect of 3D fractional-order Liu chaotic system and 3D fractional-order Li chaotic system is presented to improve the PLS of the UAV-to-ground communication network to boost the safety of OFDM downlink and the performance in terms of BER and minimise multi-user interference. Faruk et al. (2023) outlined an approach for enhancing PLS, security of a network, and BER with a small Peak-to-Average Power Ratio (PAPR) for non-terrestrial networks utilising an unidentified area vehicle. They have developed a MIMO-NOMA system that utilises the cyclic prefixed Orthogonal Variable Spreading Factor (OVSF) for encoding.

Yin et al. (2024) investigated the possibility of using UAVs to enhance the secrecy performance of uplink broadcasts in satellite supported IoT networks. In order to secure uplink communication and reduce the possibility of ground eavesdroppers capturing uplink transmissions, they first used UAV-assisted frameworks in their research. Then, they created an optimisation problem for the max-min secrecy rate with uplink power limitations. Zhai et al. (2022) addressed the simultaneous usage of Unmanned Aerial Vehicles (UAVs) and RIS in the area of Mobile Edge Computing (MEC) to enhance the environment for data interchange. They examined a unique UAV-mounted RIS-assisted MEC system, in which a UAV-mounted RIS was deployed to aid ground users' communication with a MEC server. The authors requested that the suggested algorithm considerably enhance the energy efficiency of the MEC system.

Yin et al. (2019b) proposed a secure downlink data transmission strategy for Mobile Users (MUs) utilising UAVs. By considering a protected zone free from eavesdropping,

the maximisation of the minimum secrecy rate was achieved through the NOMA technique for MUs. Adopting a frequency domain NOMA scheme, the physical layer security of satellite downlink transmission was investigated by Yin et al. (2019a). Also, a multi-user cooperative scheme was proposed to maximise the secrecy rate and enhance the spectrum efficiency of the system. Singh et al. (2022) examined a NOMA-enabled multi-user wireless communication network that used a hybrid aerial Full-Duplex (FD) transmission consisting of a RIS mounted above an FD UAV relay to provide the simultaneous flow of information from the Base Station (BS) to all ground users. Using both RCG and iterative methods, the passive beamforming of RIS and the location of RIS/UAV were concurrently optimised, and the efficacy of the suggested techniques was validated by extensive computer simulations. Abualhayja'a et al. (2021) compared the performance of RIS-enabled UAV-assisted communications to Decode-and-Forward (DF) relaying. The number of RIS components necessary to surpass DF relaying in terms of feasible rate was measured by their research. In addition, the authors demonstrated the impact of UAV altitude on the overall transmit power. Table 1 provides a brief overview of the most recent NOW approach with the proposed system model.

1.2 Contribution and organisation

According to current research, academia and industry are developing several numerologies-supported orthogonal/non-orthogonal signalling approaches for 6G wireless communication networks. This study emphasises building a multi-antenna, 6G-compatible, multi-user NOW transceiver based on RIS with UAV. The following is a summary of the study's main contributions:

- We present a unique downlink multi-user NOW transceiver UAV-mounted RIS system and signal model.
- An approach for non-orthogonal communication that combines discrete Fourier transform spreading orthogonal frequency division multiplexing (DFT-s-OFDM) and Faster-Than-Nyquist (FTN) signalling has been developed.
- We introduce a Gram Schmidt Orthogonalisation (GSO) and QR decomposition-based Multi-User MIMO (MU-MIMO) pre-coding scheme for Multi-User Interference (MUI) minimisation, which reduces the computational cost of a pre-coding approach.
- Numerical results show that the RIS-aided UAV system performs better in terms of energy efficiency and spectral efficiency. The proposed system introduces several signal detecting techniques and channel coding to give negligible Bit Error Rate (BER) performance.

The rest of this research article is organised as follows. The system model of our proposed mmWave downlink UAV mounted RIS-based multi-user NOW transceiver system is presented in Section 2, along with a description of the network model, a block diagram, channel model, signal model, signal detection and performance metric. Simulation findings are presented and discussed in Section 3. Section 4 winds up with summary thoughts.

Table 1 Comparison of the existing literature on NOW technique with proposed system model

	Proposed work	*Liu et al. (2020)*	*Asmoro and Shin (2022)*	*Sadique et al. (2022)*	*Faruk et al. (2023)*	*Yin et al. (2024)*	*Zhai et al. (2022)*	*Yin et al. (2019b)*	*Yin et al. (2019a)*
UAV-aided communication	✓	✓	✓	✓	✓	✓	✓	✓	✓
RIS-assisted network	✓	✓	✓	×	×	×	✓	×	×
Multi-user	✓	✓	✓	✓	✓	✓	×	✓	✓
Signal detection schemes	✓	×	✓	✓	×	×	×	×	×
Channel coding techniques	✓	×	✓	✓	×	×	×	×	×
Interference reduction strategy	✓	✓	✓	✓	✓	✓	×	✓	✓
Maximising achievable spectral efficiency	✓	×	×	×	×	×	×	×	✓
Maximising achievable energy efficiency	✓	×	×	×	✓	×	×	×	×
BER performance	✓	✓	✓	✓	×	×	×	×	✓

2 System model

2.1 Network descriptions

Figure 1 depicts a layout for mmWave signal transmission utilising a RIS-mounted UAV-based multi-user NOW transceiver system. One GBS, one RIS-mounted UAV and k Ground Users (GUs) are taken into account in this kind of downlink RIS-mounted UAV-based terrestrial cellular networking. Moreover, each GU is equipped with multiple antennas. The altitude of the UAV remains constant. A UAV equipped with a RIS assists in transmitting signals from a GBS to a GU. This occurs when the GU is unable to interact with the GBS due to factors such as a significant distance, barriers or a crucial position. A unique communication mechanism is used for transferring mmWave signals, and this approach is achieved through the utilisation of the RIS and each component that makes up the RIS. An inexpensive sub-wavelength programmable meta-material particle provides an extra communication connection. By exploiting these channels, the RIS is able to provide an extra spatial variety gain. This technology significantly enhances the effectiveness of mmWave communications, particularly in dense urban environments

that may obstruct direct LOS paths. This not only extends the GBS's range, but also improves the reliability and quality of the communication links to the GUs. The multiple antennas at each GU, in conjunction with the spatial diversity the RIS gains, guarantee a more stable and high-throughput communication network. Basically, this method uses the special features of RIS and UAV technology to get around the problems that come with sending mmWave signals, like high path loss and being sensitive to obstacles. This makes it possible for faster and more reliable wireless communication networks.

Figure 1 Multi-user NOW transceiver system scenario at mmwave (see online version for colours)

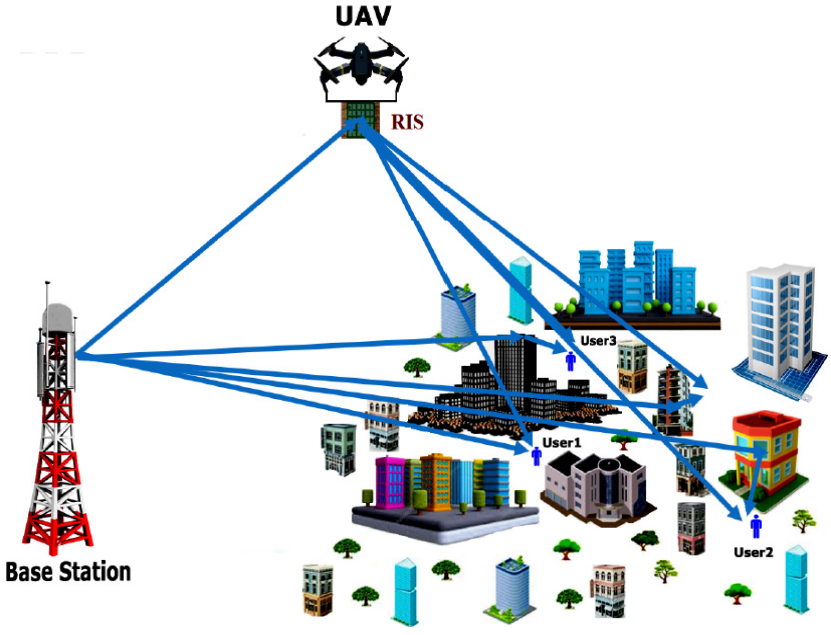

2.2 Schematic diagram

Figure 2 is a conceptual block diagram of the RIS-mounted, UAV-based, multi-user NOW transceiver structure. It illustrates that k users are presumed to secure their own transmitted data as synthetically generated binary data and that the binary data of each user is sent up along the channel encoder first and then through a digital modulator to make the complex symbols (Vitetta et al., 2013; Jiang, 2010; Rappaport, 2002). The complicated digitally modulated symbols are put into blocks, and DFT spreading is done on each block. In centralised subcarrier mapping, null subcarriers (zero-paddings) are added to both ends of the data subcarriers after the DFT-spread complex symbols are mapped into the required number of subcarriers in the frequency bandwidth (Tanangsanakool et al., 2020). OFDM is used to modulate the complex symbols that are mapped to a central subcarrier in blocks, and each block of data is cyclically prepended and then processed for FTN modulation (Liu et al., 2020). Complex data that has been modulated with FTN is reshaped and pre-coded with a transmit pre-coding scheme that depends on the channel (Wu et al., 2014). From the GBS, the pre-coded signal data of

each user is added up, scaled to the desired transmission power and sent to both GUs and RIS. At each user's receiving end, linear signal detection schemes like Zero Forcing, MMSE, CD-based ZF and LR-MMSE are used to find all the transmitted signals (Gangarajaiah et al., 2017; Bai and Choi, 2012). After removing cyclic prefixing, the FTN demodulation of each user's signal and then OFDM demodulation is done. The free cyclic prefix OFDM demodulated signal is given a subcarrier demapping scheme and then DFT dispreading is used to process it further. The DFT-peeled signal is sent through a digital demodulator and a channel decoder, and then the binary data that were sent are finally retrieved.

Figure 2 Block diagram of a multi-user NOW transceiver for RIS-assisted UAV communication (see online version for colours)

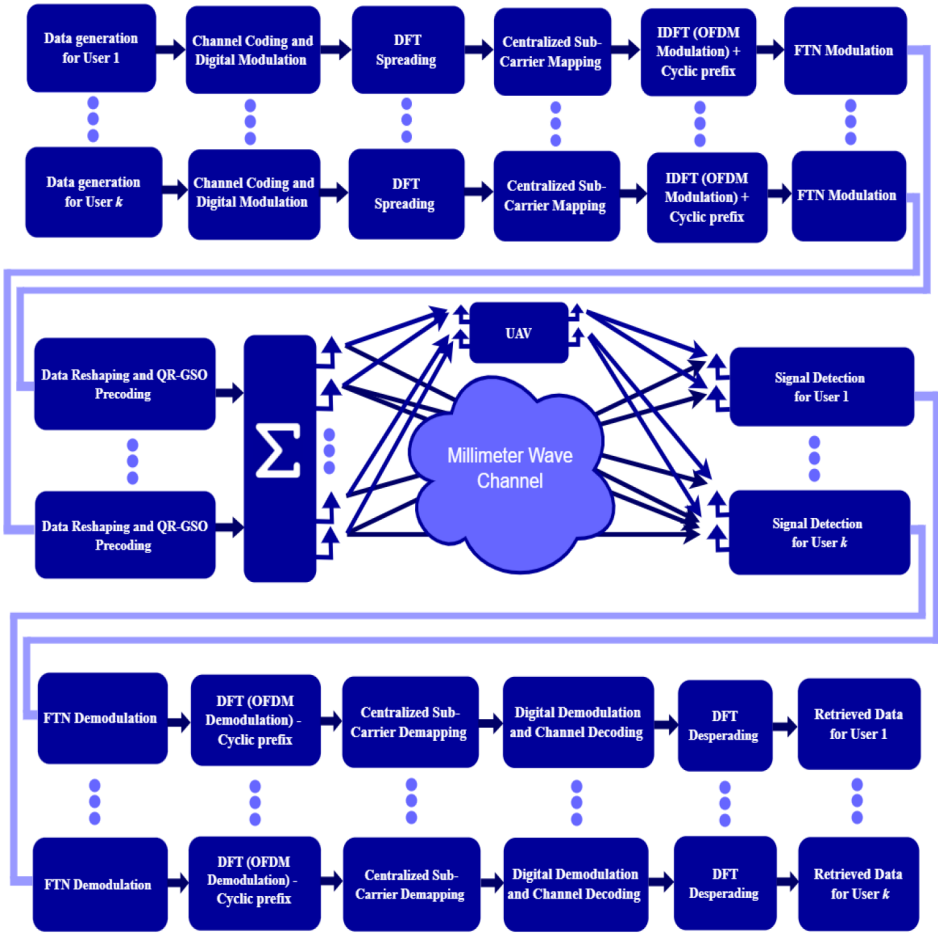

2.3 Channel model

A probabilistic LOS/NLOS mixture Path Loss (PL) model has been added to our analysis for both the GBS to GUs and the UAV-mounted RIS to GUs links. A probabilistic LOS

model is taken into account when uplink transmission from the ground BS to UAV-mounted RIS is involved. The probability condition-based mixed PL model for LOS and NLOS links between ground BSs to GUs and RIS placed on UAVs can be expressed as follows:

$$PL_{AVG-k}^{UAV} = P\left(LOS\right)_k^{UAV} PL\left(LOS\right)_k^{UAV} + \left[1 - P\left(LOS\right)_k^{UAV}\right] PL\left(NLOS\right)_k^{UAV} \quad (1)$$

$$PL_{AVG-k}^{GBS} = P\left(LOS\right)_k^{GBS} PL\left(LOS\right)_k^{GBS} + \left[1 - P\left(LOS\right)_k^{GBS}\right] PL\left(NLOS\right)_k^{GBS} \quad (2)$$

where PL_k^{UAV} indicates the average path loss in the form of dB from UAV-mounted RIS to GUs links ((1)) and PL_k^{GBS} represents the mean path loss in dB from GBS to GUs links. $P\left(LOS\right)_k^{UAV/GBS}$, $PL\left(LOS\right)_k^{UAV/GBS}$ and $PL\left(LOS\right)_k^{UAV/GBS}$ are the LOS probabilities of UAV-mounted RIS/GBS to GU k, LOS PL of UAV-mounted RIS/GBS to GU k in dB and NLOS PL of UAV-mounted RIS/GBS to GU k in dB, respectively. The $PL\left(LOS\right)_k^{UAV/GBS}$ and $PL\left(LOS\right)_k^{UAV/GBS}$ can be written in terms of distance $d_k^{UAV/GBS}$ between UAV/GBS and the GU k

$$PL\left(LOS\right)_k^{UAV/GBS} = 20\log_{10}\left(d_k^{UAV/GBS}\right) + 20\log_{10}\left(f_c\right) + 20\log_{10}\left(4\pi / c\right) + \eta_{LOS} \quad (3)$$

$$PL\left(NLOS\right)_k^{UAV/GBS} = 20\log_{10} d_k^{UAV/GBS} + 20\log_{10}\left(f_c\right) + 20\log_{10}\left(4\pi / c\right) + \eta_{NLOS} \quad (4)$$

where $d_k^{UAV/GBS}$ presents the length (m) between the UAV-mounted RIS/GBS and GU k, f_c defines the carrier frequency (Hz), c denotes the light's speed (m/sec), η_{LOS} and η_{NLOS} (3 dB and 23 dB) from Saad et al. (2020) are denoting the excessive coefficients PL for LOS and NLOS links. The probability of having a LOS link between the UAV-mounted RIS/GBS and the GU k in a dense urban area can be stated as:

$$P\left(LOS\right)_k^{UAV/GBS} = \prod_{n=1}^{m}\left[1 - \exp\left(-\frac{\left[h_{UAV/GBS} - \left(n + \frac{1}{2}\right)\left(h_{UAV/GBS} - h_k\right)/\left(m+1\right)\right]^2}{2\Omega^2}\right)\right] \quad (5)$$

where $m = \text{floor}(r\sqrt{\varsigma\xi})$, r is the horizontal length (km) from the UAV-mounted RIS/GBS to the GU k, $\varsigma(= 0.5)$ is the ratio of the built-up to the entire land area and $\xi(= 300)$ is the average number of buildings in every single unit area (km^2) and $\omega(= 20)$ is a scale parameter that describes the height distribution of the buildings' according to the Rayleigh probability density function. The mean path loss having both LOS and NLOS link between the UAV/GBS and the GU k in dense urban area can be written as (Sabuj et al., 2023, 2022):

$$\begin{aligned} PL\left(AVG\right)_k^{UAV/GBS} &= P\left(LOS\right)_k^{UAV/GBS} PL\left(LOS\right)_k^{UAV/GBS} \\ &+ \left[1 - P\left(LOS\right)_k^{UAV/GBS}\right] PL\left(NLOS\right)_k^{UAV/GBS} \end{aligned} \quad (6)$$

In case of linking the GBS to UAV mounted RIS, the $PL\left(LOS\right)_{GBS}^{UAV}$ and $PL\left(NLOS\right)_{GBS}^{UAV}$ can be expressed in terms of length d_{GBS}^{UAV} between UAV and GBS

$$PL\left(LOS\right)_{GBS}^{UAV} = 20\log_{10}\left(d_{GBS}^{UAV}\right) + 20\log_{10}\left(f_c\right) + 20\log_{10}\left(4\pi / c\right) + \eta_{LOS} \tag{7}$$

$$PL(NLOS)_{GBS}^{UAV} = 20\log_{10}(d_{GBS}^{UAV}) + 20\log_{10}(f_c) + 20\log_{10}(4\pi / c) + \eta_{NLOS} \tag{8}$$

The probability of having a LOS link between the UAV-mounted RIS and the GBS in dense urban area can be written as

$$P\left(LOS\right)_{GBS}^{UAV} = \prod_{n=1}^{m}\left[1 - \exp\left(-\frac{\left[h_{UAV} - \left(n+\frac{1}{2}\right)\left(h_{UAV} - h_{GBS}\right)/\left(m+1\right)\right]^2}{2\Omega^2}\right)\right] \tag{9}$$

The mean path loss having both LOS and NLOS link between the UAV and the GBS in dense urban area can be written as (Sabuj et al., 2023, 2022)

$$PL\left(AVG\right)_{UAV}^{GBS} = P\left(LOS\right)_{UAV}^{GBS} PL\left(LOS\right)_{UAV}^{GBS} + \left[1 - P\left(LOS\right)_{UAV}^{GBS}\right] PL\left(NLOS\right)_{UAV}^{GBS} \tag{10}$$

The estimated power of complex MIMO fading channel linking the GBS to the GU k can be expressed as

$$\bar{H}_k = \sqrt{\left(\frac{ChPo_{GBSk}}{2}\right)\left[\text{randn}\left(L,M\right) + \sqrt{-1}\text{randn}\left(L,M\right)\right]} \tag{11}$$

where $ChPo_{GBSk} = 10^{-PL(AVG)_k^{GBS}/10}$.

The estimated power of complex MIMO fading channel linking the GBS to the UAV-mounted RIS can be expressed as

$$H_o = \sqrt{\left(\frac{ChPo_{GBSUAV}}{2}\right)\left[\text{randn}\left(N,M\right) + \sqrt{-1}\text{randn}\left(N,M\right)\right]} \tag{12}$$

where $ChPo_{GBSUAV} = 10^{-PL(AVG)_{UAV}^{GBS}/10}$.

The estimated power of complex MIMO fading channel linking between the UAV-mounted RIS and the GU k can be written as

$$H_{UAV-k} = \sqrt{\left(\frac{ChPo_{UAVk}}{2}\right)\left[\text{randn}\left(M,N\right) + \sqrt{-1}\text{randn}\left(M,N\right)\right]} \tag{13}$$

where $ChPo_{UAVk} = 10^{-PL(AVG)_k^{UAV}/10}$.

The equivalent channel for GU k from GBS to GU k in direct transmission and additional transmission via UAV-mounted RIS to GU k can be stated as:

$$H_k = \bar{H}_k + H_{uav-k}\bar{\Psi}H_o \tag{14}$$

where $\bar{\Psi}$ is a $N \times M$ diagonal matrix and it is defined as $\bar{\Psi} = \left[\beta_1 e^{j\theta_1}, ..., \beta_N e^{j\theta_N} \right]$ with j denoting imaginary. $\theta_n \in [0, 2\pi]$ and $\beta_n \in [0,1]$ denote the phase shift and amplitude reflection coefficient of the *n*-th element of IRS, respectively.

2.4 Signal model

For GU k, the vector of binary data b_k is channel encoded to create a new binary data vector c_k with data length N_1, and the c_k is further turned into a digitally modulated complex symbol vector x_k with data length N_2. The data vector x_k is reorganised into the pre-DFT spreading block, $\bar{X}_k$, has the dimensions $\bar{K} \times \bar{M}$ matrices. The number of data samples in each column of the matrix $\bar{X}_k$ is $\bar{K}$, and the number of pre-DFT spread column vectors is $\bar{M}$. The spreading size of the DFT represents the symbol $\bar{K}$. The $\bar{m}$-th discrete frequency domain DFT spread signal vector for the GU k with $\bar{n}$-th frequency domain sample index and $\tilde{n}$-th time domain sample index can be stated in terms of considering various elements of the matrix, $\bar{X}_k$ containing digitally modulated complex symbols as

$$\bar{\bar{X}}_{k,\bar{m}}[\bar{n}] = \sum_{\tilde{n}=1}^{\tilde{n}=\bar{K}-1} \bar{X}_{k,\bar{m}}[\tilde{n}] e^{\frac{j2\pi\tilde{n}\bar{n}}{\bar{K}}} \tag{15}$$

where $\bar{n} = 0,1,2,3,...,\bar{K}-1$, $k = 1,2,3,4,...$, $\bar{m} = 1,2,...,\bar{M}$ and $\tilde{n} = 0,1,2,...,\bar{K}-1$, respectively. In centralised subcarrier mapping, N_0 is the number of zeros to be added in equal numbers at both ends of the DFT spread signal vector of matrix $\bar{\bar{X}}_k$ and $\bar{N} = \bar{K} + 2N_0$ is the total number of data samples in properly designed centrally sub carrier mapped input data matrix, $\bar{\bar{\tilde{X}}}_k$ and $\bar{N}$ is denoted by the IDFT size and the matrix $\bar{\bar{\tilde{X}}}_k$ is of $\bar{N} \times \bar{M}$ in size. The discrete time domain IDFT operated/OFDM modulated signal vector with $\hat{n}$-th time-domain sample index and $\bar{\bar{n}}$-th sub carrier index for GU k can be stated as:

$$\bar{\bar{\tilde{X}}}_{k,\bar{m}}[\hat{n}] = \frac{1}{N} \sum_{\bar{\bar{n}}=0}^{\bar{\bar{n}}=\bar{N}-1} \bar{\bar{X}}_{k,\bar{m}}\left[\bar{\bar{n}}\right] e^{-\frac{j2\pi\hat{n}\bar{\bar{n}}}{\bar{N}}} \tag{16}$$

where $\hat{n} = 0,1,2,...,\bar{N}-1$, $\bar{\bar{n}} = 0,1,2,...,\bar{N}-1$, $k = 1,2,3,4,...$ and $\bar{m} = 1,2,...,\bar{M}$. With cyclic prefixing of sample length N_{CP}, the cyclic prefixed IDFT operated/OFDM modulated signal vector can be written as:

$$\bar{\bar{\tilde{X}}}_{k,\bar{m}}\left[\hat{n}\right] = \begin{bmatrix} \bar{\bar{\tilde{X}}}_{k,\bar{m}}\left[\hat{\tilde{n}}\right] \\ \bar{\bar{\tilde{X}}}_{k,\bar{m}}\left[\hat{\tilde{n}}\right], \end{bmatrix} = \begin{bmatrix} \frac{1}{N} \sum_{\tilde{\tilde{n}}=\bar{N}-N_{CP}}^{\tilde{\tilde{n}}=\bar{N}-1} \bar{\bar{X}}_{k,\bar{m}}[\tilde{\tilde{n}}] e^{-\frac{j2\pi\tilde{\tilde{n}}\hat{\tilde{n}}}{\bar{N}}} \\ \frac{1}{N} \sum_{\tilde{\tilde{n}}=\bar{N}-N_{CP}}^{\tilde{\tilde{n}}=\bar{N}-1} \bar{\bar{X}}_{k,\bar{m}}[\bar{\bar{n}}] e^{-\frac{j2\pi\hat{n}\bar{\bar{n}}}{\bar{N}}} \end{bmatrix} \tag{17}$$

where $\hat{n} = 0,1,...,\left(\bar{N} + N_{CP}\right) - 1$, $\bar{\bar{n}} = 0,1,2,...,\bar{N} - 1$, $\tilde{\tilde{n}} = \left(\bar{N} + N_{CP}\right),...,\bar{N} - 1$, $\bar{\bar{n}} = 0,1,2,3,..,\bar{N} - 1$, $\hat{\hat{n}} = \left(\bar{N} + N_{CP}\right),...,\bar{N} - 1$, $\hat{n} = 0,1,2,...,\bar{N} - 1$. The cyclic prefixed OFDM modulated signal matrix $\breve{\breve{X}}_k$ is of $\ddot{N} \times \bar{M}$ in size, where $\ddot{N} = \bar{N} + N_{CP}$.

Each column-wise signal vector in the matrix $\breve{\breve{X}}_k$ is up sampled in the FTN modulation with an up sampling factor of R(=4), and a new data matrix $\dddot{X}_k$ of size $\dddot{N} \times \bar{M}$ is created, where $\dddot{N} = R \times \ddot{N}$. Each of the $\bar{m}$-th signal vectors of the matrix $\dddot{X}_k$ receives an application of a root raised cosine pulse shaping filter (Sadique et al., 2021). Such a root raised cosine pulse shaping filter's response can be expressed as:

$$h_{SRC}(s) = \frac{\left[\frac{4\alpha}{\pi}\left(\frac{\cos\left(1+\alpha\right)\pi s}{r}\right)\right] + \left[\left(1-\alpha\right)\left(\frac{\sin(1-\alpha)\pi s}{r}\right)\right]}{\sqrt{r}\left[1-\left(\frac{4\alpha s}{r}\right)^2\right]} \tag{18}$$

where α(= 0.25) is the roll off factor. In such filter, it is assumed that its impulse response is truncated over Ω(= 6) quantity of symbols and the range of the filter coefficient is $\left(r\Omega + 1\right)$ and the sample index number, s used in Equation ((18)) is defined by $s = 0,1,2,3,...,r\Omega$. The FTN modulated signal can be stated as:

$$\dddot{X}_{k,\bar{m}}[\dddot{n}] = \dddot{X}_k\left[\hat{n}\right] \otimes h_{SRC}(s) \tag{19}$$

where the symbol $\otimes$ is indicative of discrete convolution operator. The length of the samples in each column wise signal vector of the matrix $\dddot{X}$ is $\dddot{N} + r\left(\Omega - 1\right) + 1$. $\dddot{n} = 0,1,2,...,\dddot{N} + r\left(\Omega - 1\right)$, $\hat{n} = 0,1,2,...,\dddot{N} - 1$. The FTN modulated signal matrix $\dddot{X}_k$ is of $\dddot{N} \times \bar{M}$ in size where $\dddot{N} = \ddot{N} + r\left(\Omega - 1\right) + 1$.

The entire matrix $\dddot{X}_k$ is layered into a single column vector and then organised into a data matrix $\dddot{X}_k$ of size $N_R \times N_c$, where N_R is the amount of receiving antennas for each GU and $N_c = \frac{\dddot{N} \times \bar{M}}{N_R}$. In purpose of reducing multi-user interference reduction, low-complexity QR-GSO pre-coding algorithm has been implemented for each GU. In such algorithm, estimated pre-coding weight for the GU k is obtained from the estimated channel presented in equation (14).

In the QR-GSO pre-coding algorithm, firstly pre-coding matrix W^a is estimated using QR decomposition of the matrix H_s^H as

$$H_S^H = QR \tag{20}$$

where $(\cdot)^H$ indicates Hermitian transformation, $Q \in C^{N_T \times KN_R}$ is an orthogonal matrix and $R \in C^{KN_R \times KN_R}$ is an upper triangular matrix. The combined channel matrix H_s with consideration of $L = R^H$ can be written as

$$H_S = LQ^H \tag{21}$$

Alternatively, the pseudo-inverse of the concatenated channel matrix H_s is computed as

$$H_S \dagger = H_s{}^H \left(H_s H_S{}^H\right)^{-1} = QR\left(LQ^H QR\right)^{-1} = QL^{-1} = Q\left[\hat{L}_1, ..., \hat{L}_k, ..., \hat{L}_K\right] \tag{22}$$

where $\tilde{L}_k \in C_T^N \times N_k$ represents the sub-matrix of $L^{-1} \in C_T^N \times N_k$ for GU k. Since $H_S \dagger H_S = I$, I being the identity matrix, we can write $\tilde{H}_k Q\hat{L}_k = 0$ and $Q\hat{L}_k$ is the MUI null space vector. To reduce processing complexity, a simplified approach for determining the inverse of L can be employed. Since L is a lower triangular matrix, it can be transformed into a unit lower triangular matrix B by multiplying it by a diagonal matrix G whose diagonal elements are the inverse of L's diagonal elements, as demonstrated by the following expression:

$$B = GL \tag{23}$$

We can determine the inverse of the matrix L by

$$L^{-1} = B^{-1}G = Q\left[\hat{L}_1, ..., \hat{L}_k, ..., \hat{L}_K\right] \tag{24}$$

It is important to note that $Q\hat{L}_k$ does not have an orthogonal basis, instead the pre-coding matrix for GU k should contain the orthogonal basis of $Q\hat{L}_k$. Thus, the GSO method is used to determine the orthogonal basis $\hat{L}_k^0$ for $\hat{L}_k$ is defined by

$$\hat{L}_k^0 = GSO\left(\hat{L}_k\right) \tag{25}$$

Given that, an orthogonal matrix is Q, the columns of $Q\hat{L}_k^0$ serve as an orthonormal basis for the null space of $\tilde{H}_k$. Consequently, for the GU k of the proposed QR-GSO pre-coding algorithm the initial pre-coding matrix $W_k{}^a$ is given as follows:

$$W_k{}^a = Q\hat{L}_k^0 \tag{26}$$

After traversing all GUs, for K GUs the initial pre-coding matrix W^a is denoted as

$$W_k{}^a = \left[W_1{}^a, ..., W_k{}^a, ..., W_K{}^a\right] \tag{27}$$

In the QR-GSO pre-coding process, a second pre-coding operation must be performed to obtain the highest pre-coding gain for every GU. In this step, the effective channel matrix H_{effk} for the GU k is formulated as

$$H_{effk} = H_k W_k^a \tag{28}$$

Using the SVD function on the effective channel matrix H_{effk}, we get

$$H_{effk} = U_K \Lambda_k V_k^H = U_K \Lambda_k \left[V_k^{(1)} V_k^{(0)} \right]^H \tag{29}$$

The value B_{effk} represents the position of H_{effk}. The formula for obtaining the second pre-coding matrix W_k^b for GU k is:

$$W_k^b = V_k^1 \tag{30}$$

After traversing each GU, the second pre-coding matrix W^b for each GU K can be expressed as follows:

$$W^b = \left[W_1^b, ..., W_k^b, ..., W_K^b \right] \tag{31}$$

The overall pre-coding matrix with application of QR-GSO pre-coding algorithm can be written as:

$$W = W^a W^b \tag{32}$$

GU k pre-coding matrix can be expressed as (Wu et al., 2014)

$$W_k = W_k^a W_k^b \tag{33}$$

Such individual QR-GSO pre-coding algorithm implemented pre-coding matrix of each GU is the size of $N_T \times N_R$ matrix. However, multiplying pre-coded data matrix $\overset{\cdots}{X}_k$ of size $N_R \times N_c$ for the GU k with the assigned pre-coding matrix W_k, we get pre-coded matrixed data for the GU k with its matrix size $N_T \times N_c$ as

$$\widetilde{X}_k = W_k \overline{X}_k \tag{34}$$

Summing all the data for all the GUs from signal model describe in equation (29), the transmitted data matrix D of size $N_T \times N_c$ can be stated as

$$D = W_k \overline{X}_k + \sum_{j=1, j \neq k}^{j=4} W_j \overline{X}_j \tag{35}$$

The MIMO fading channels for GUs can be taken into account using equation (14), and the whole MIMO channel matrix for K GUs is expressed as

$$H_s = \left[\bar{H}_1^T, \bar{H}_2^T, ..., \bar{H}_K^T \right]^T \tag{36}$$

In case of considering the total amount of transmitting antennas $\left(N_T\right)$ at the ground station and receiving antennas $\left(N_R\right)$ for every GU, the total channel matrix $\bar{H}_s$, eliminating the *k*-th GU's channel, is given by

$$\bar{H}_k = \left[\bar{H}_1^T, \bar{H}_{k-1}^T, \bar{H}_{k+1}^T, ..., \bar{H}_K^T \right]^T \tag{37}$$

where $\bar{H}_k \in C^{\tilde{N}_k \times N_T}$, $\tilde{N}_k = KN_R - N_R$.

Considering signal transmission in all time slots, at the GU k the accepted signal can be written as

$$Y_k = H_k D = H_k\left(W_k \overline{X}_k + \sum_{j=1, j\neq k}^{j=4} W_j \overline{X}_j\right) + n_k = H_k\left(W_k \overline{X}_k\right) + H_k \sum_{j=1, j\neq k}^{j=4} W_j \overline{X}_j + n_k \quad (38)$$

where $n_k \sim \mathbb{CN}\left(0_{NR}, \sigma_k^2 I_{N_R \times N_R}\right)$ represents additive white Gaussian noise (AWGN) and all terms in equation (38) reflect $N_R \times N_c$ sized matrix data.

2.5 Signal detection

In case of $k \neq j$, $H_k W_j$ would be 0. Thus, equation (38) can be stated as

$$Y_k = H_k\left(W_k \overline{X}_k\right) + n_k = \hat{H}_k \overline{X}_k + n_k, \quad (39)$$

where modified form of channel matrix for the GU k is $\hat{H}_k \left(= H_k W_k\right)$. With application of various signal detection techniques addressed at Gangarajaiah et al. (2017) and Bai and Choi (2012), using Zero Forcing (ZF) signal detection technique and its applicability to signal model of equation (39), for the GU k the detected signal can be written as

$$\hat{X}_{k:ZF} = \hat{H}_k \left(\hat{H}_k{}^H \hat{H}_k\right)^{-1} Y_k \quad (40)$$

Using the Minimum Mean Square Error (MMSE) technique for signal detection, for GU k the detected signal can be stated as

$$\hat{X}_{k:MMSE} = \hat{H}_k \left(\hat{H}_k{}^H \hat{H}_k + \frac{N_0}{E_s}\right)^{-1} Y_k \quad (41)$$

where E_s denotes the symbol energy and N_0 denotes noise power spectral density. If Cholesky Decomposition (CD)-based ZF signal detection is applicable, the detected signal for GU k can be defined as

$$\hat{X}_{k:CD-ZF} = \left(L_k^H\right)^{-1} \left(L_k\right)^{-1} \hat{H}_k^H Y_k \quad (42)$$

where L_k is the lower triangular matrix acquired from CD of matrix $\left(\hat{H}_k^H \hat{H}_k\right)$. In case of applicability of Lattice Reduction-based MMSE (LR-MMSE) signal detection technique. The observed signal for GU k with implementation of LR-MMSE technique for signal detection can be written as

$$\widehat{X}_{k:LR-MMSE} = \left(\widehat{U}_k\right)^{-1} \left(\widehat{G}_k{}^H \widehat{W}_k + \frac{N_0}{E_s} \widehat{U}_k^{-H} \widehat{U}_k^{-1}\right)^{-1} \widehat{G}_k{}^H Y_k \quad (43)$$

The data matrix for the GU k estimated from all the detected signals of equations (40), (41), (42) and (43) are of $N_R \times N_c$ matrix in size. Ignoring the nomenclature of the signal detection technique and identifying detected signal as $\hat{X}_k$, its all elements can be

layered into a single column of $\tilde{\tilde{b}}_k$ vector and it is organised into a matrix $\tilde{\tilde{\tilde{X}}}_k$ with the dimension of $\dddot{N} \times \bar{M}$. The signal model expressed in equation (21) ratifies itself as real, symmetric and linearly phased, it can be used effectively as matched filter and on implementation of such match filter to de-convolved every column wise signal of $\tilde{\tilde{\tilde{X}}}_k$ vector matrix and further implementation of down sampling with identical sampling factor R , we get retrieved FTN demodulated signal matrix $\ddot{\bar{X}}_k$ of $\ddot{N} \times \bar{M}$ in size. On execution of various necessary steps OFDM demodulation, Centralised sub-carrier demapping, DFT dispreading, etc., retrieved data of the GU k will be available.

2.6 Performance metric

From equation (38), we can figure out the Signal-to-Interference-plus-Noise Ratio (SINR) for the GU k

$$SINR_k \triangleq \frac{\frac{1}{N_R NC}\left\| H_k \left(W_k \bar{X}_k \right) \right\|^2}{\frac{1}{N_R NC}\left\| H_k \sum_{j=1, j\neq k}^{j=4} W_j \bar{X}_k \right\|^2 + \sigma_k^2} \tag{44}$$

where σ_k^2 is a variance. The system spectral efficiency, R_{SE} (bps/Hz) in terms of $SINR_k$ can be expressed as

$$R_{SE} \triangleq \sum_{k=1}^{k=4} \log_2\left(1 + SINR_k\right) = \sum_{k=1}^{k=4} \log_2 \left(1 + \frac{\frac{1}{N_R NC}\left\| H_k \left(W_k \bar{X}_k \right) \right\|^2}{\frac{1}{N_R NC}\left\| H_k \sum_{j=1, j\neq k}^{j=4} W_j \bar{X}_k \right\|^2 + \sigma_k^2} \right) \tag{45}$$

The energy efficiency, η_{EE} (bits/Joule) for our proposed multi-user downlink UAV mounted RIS-assisted NOW transceiver system can be written as

$$\eta_{EE} = \frac{B_W R_{SE}}{\varsigma P_{TR} + P_{BS} + K P_{UE} + N P_n\left(b\right)} \tag{46}$$

where B_W denotes transmission bandwidth, R_{SE} denotes the system spectral efficiency, $\xi (= 1.2)$ is the circuit dissipated power coefficients at base station, ρ_{TR} is the average transmit power, $P_{UE}\left(= 10dBm\right)$ is the power that has been lost at each GU, $P_n(b)\left(= 10dBm\right)$ is the diminished power at the n-th RIS element, N is the total quantity of RIS reflecting elements and $P_{BS}\left(= 10dBW\right)$ is the static power consumption/circuit dissipated power (Huang et al., 2019; You et al., 2020).

3 Simulation results

This section presents and analyses numerical findings for a downlink UAV-mounted multi-user NOW transceiver system that was processed using the parameters of simulation listed in Table 2. In this case, a unique scenario with four users – whose number is increasing – is taken into consideration. In this study, it is assumed that everyone is aware of the locations of the four terrestrial GUs and the UAV. The GUs typically need to estimate the CSI. In reality, the CSI of the channels between the GBS and the GUs and that of the channels between the GBS and the RIS mounted on the UAV can vary. The probabilistic LOS/NLOS mixture path loss model discussed at Al-Hourani et al. (2014) is taken into consideration in this instance, and CSI can be produced in particular circumstances of downlink transmission from the predicted MIMO flat fading channel. At the receiver, these estimated channels are used for channel equalisation and signal detection. At the transmitter, they are used for transmit pre-coding.

Table 2 Simulation parameters

Parameter	*Value*
Input data type	Synthetically generated binary data
Digital modulation	16 QAM
Channel coding	RA and LDPC
Subcarrier spacing (kHz)	120
Carrier frequency (GHz)	39
No of transmitting antennas of GNB	8
No of active physical resource blocks in each OFDM symbol	275
DFT spreading size	792
IDFT size	4096
Transmission Bandwidth (MHz)	396
No of RIS elements	25, 50 and 75
Height of RIS mounted UAV from ground surface (m)	200
No of receiving antennas of each GU	2
Modulation	16 QAM

Figure 3 shows the average receive signal power (the GU's own targeted signal plus the MUI signal) when the median transmit power is changed from 0 to 50 dBm (1 to 100 mW). The respective distances between the GBS and GUs (k=1, 2, 3 and 4) are 115.79 m, 125.71 m, 151.17 m and 174.51 m. The UAV-mounted RIS is at 200 m height above the earth surface. All the GUs are receiving signals both directly and via UAV-mounted RIS transmission. Owing to the fact that 37 GHz mmWave signal transmission is taken into account, it significantly affects the signal strength that is received.

Figure 3 Estimated average receive signal power versus average transmit power for a multi-user UAV-mounted RIS-assisted NOW transceiver (see online version for colours)

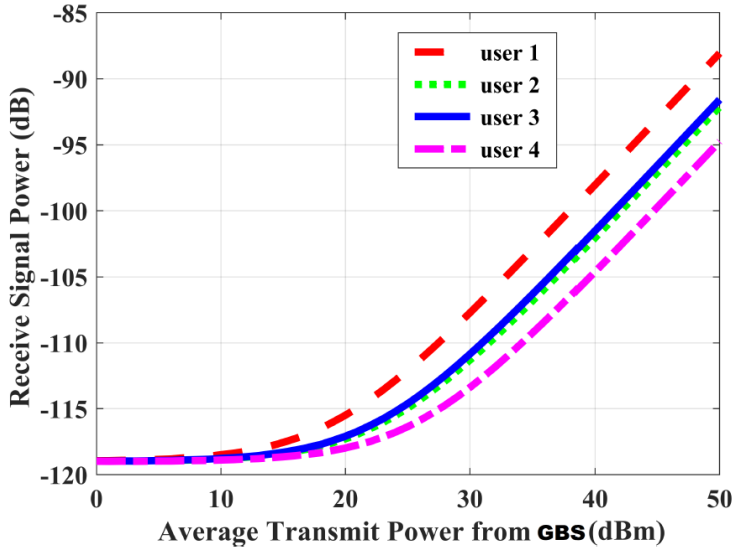

Figure 4 shows the estimated received SINR that can be reached with different average transmit powers. It also shows that the signal attenuation at 37 GHz mmWave transmission is very large, and the existence of interference signals causes the SINR values for every GU to decrease.

Figure 4 Achievable receive SINR versus average transmit power for multi-user UAV-mounted RIS-assisted NOW transceiver (see online version for colours)

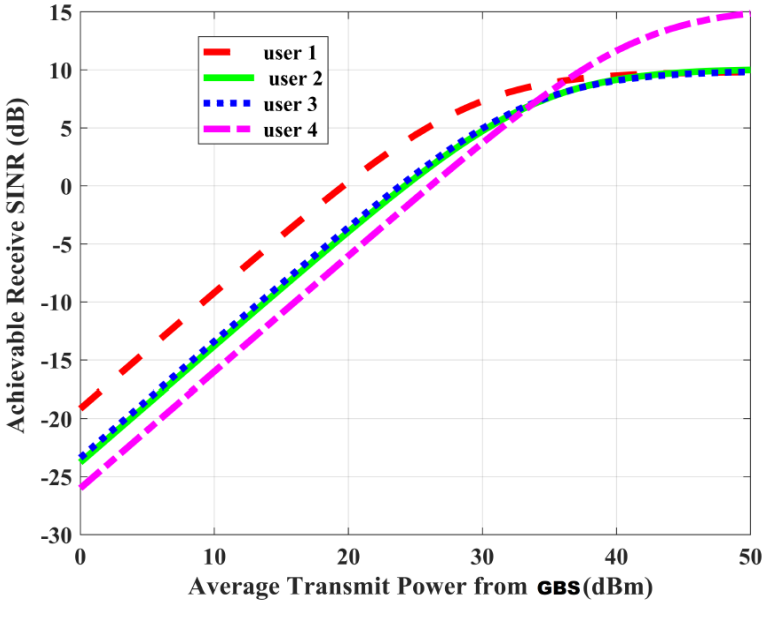

Figure 5 presents the estimated Cumulative Distribution Function (CDF) of the SINR received by all four GUs when a RIS mounted on a UAV flying 200 m above the ground surface is taken into account. Figure 7 shows that the SINR CDF change a lot depending on where the GU is in relation to the serving RIS on the UAV and the GBS. The SINR value for GU 1 is 10.86 dB; the SINR value for GU 2 is 9.06 dB; the SINR value for GU 3 is 8.20 dB and the SINR value for GU 4 is 5.45 dB. This indicates that the suggested technique's four GUs can communicate with SINR values that vary from 10.86 dB to 5.45 dB.

Figure 5 Receiving SINR CDF for a multi-user UAV-mounted RIS-assisted NOW transceiver (see online version for colours)

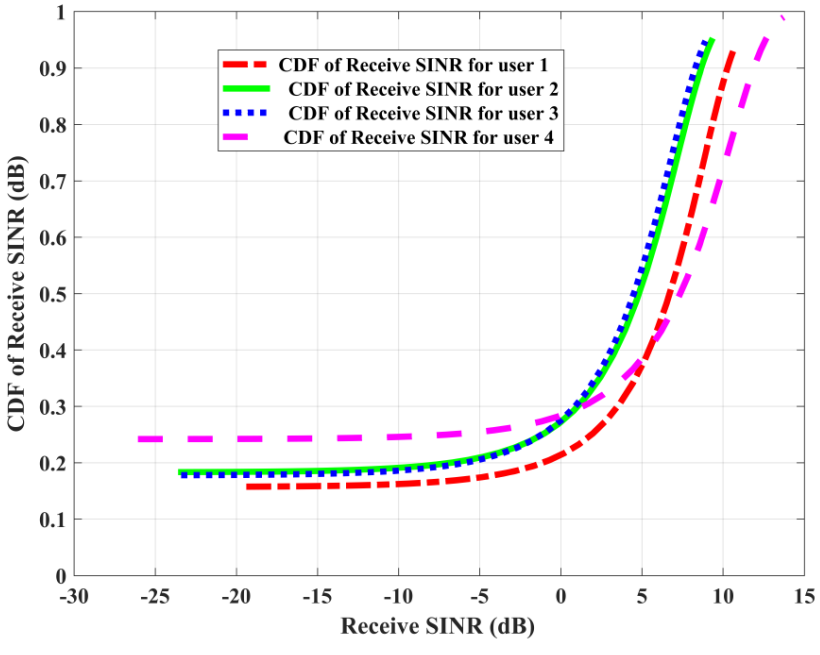

Figure 6 shows the estimated achievable spectral efficiency values for various average transmit powers with varying heights of UAV-mounted RIS. It is noticeable from the graphs in Figure 6 that both transmit power and the height of the UAV-mounted RIS have a significant impact on achieving maximum spectral efficiency of the system. Since the UAV height increases, the spectral efficiency decreases. This is because path loss increases as distance increases.

Figure 7 shows the estimated achievable spectral efficiency values that can be reached when different transmit powers and the total amount of RIS passive elements are considered. Given the lower number of RIS passive elements, it is clear that the simulated system has good spectral efficiency in this situation.

Figure 6 Achievable spectral efficiency versus average transmit power for varying the height of the UAV in a multi-user UAV-mounted RIS-assisted NOW transceiver (see online version for colours)

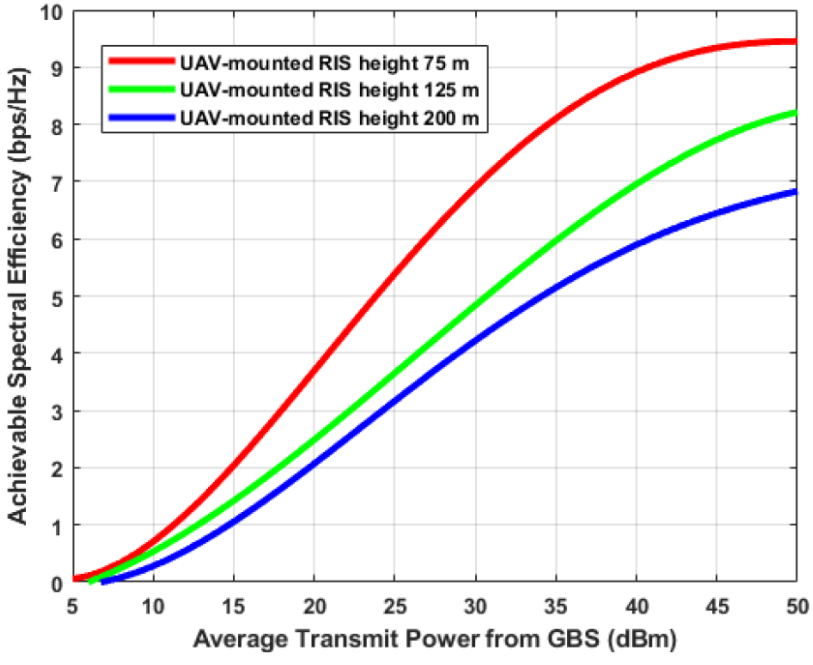

Figure 7 Achievable spectral efficiency versus average transmit power for varying the number of RIS passive elements in a multi-user UAV-mounted RIS-assisted NOW transceiver (see online version for colours)

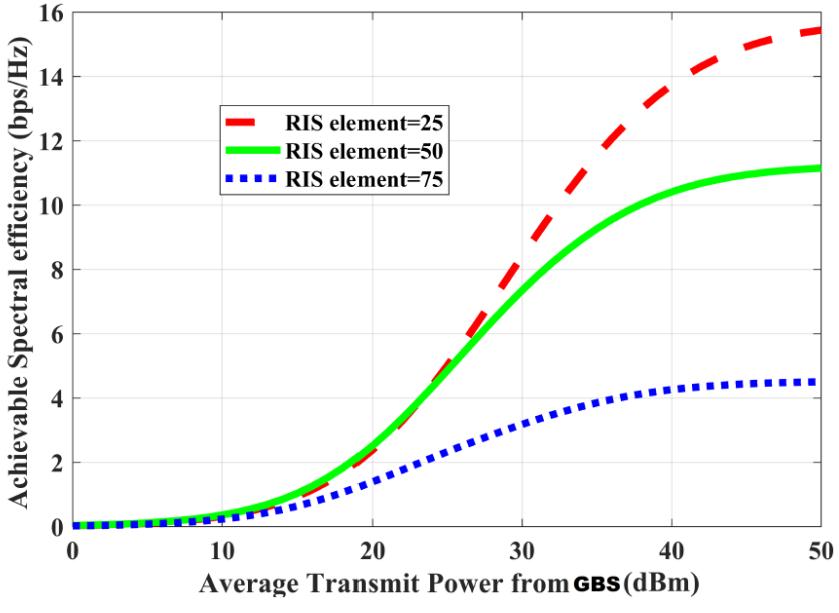

Figure 8 illustrates the energy efficiency performance of the designed system. The energy efficiency performance saturates at the specified GBS transmit power. It is not monotonically increasing with the increase in GBS transmit power. It is clear that the best use of energy happens at 39 dBm, 37 dBm and 37 dBm when there are 25, 50 and 75 RIS elements.

Figure 8 Average energy efficiency versus average transmit power for varying the number of RIS elements in a multi-user UAV-mounted RIS-assisted NOW transceiver (see online version for colours)

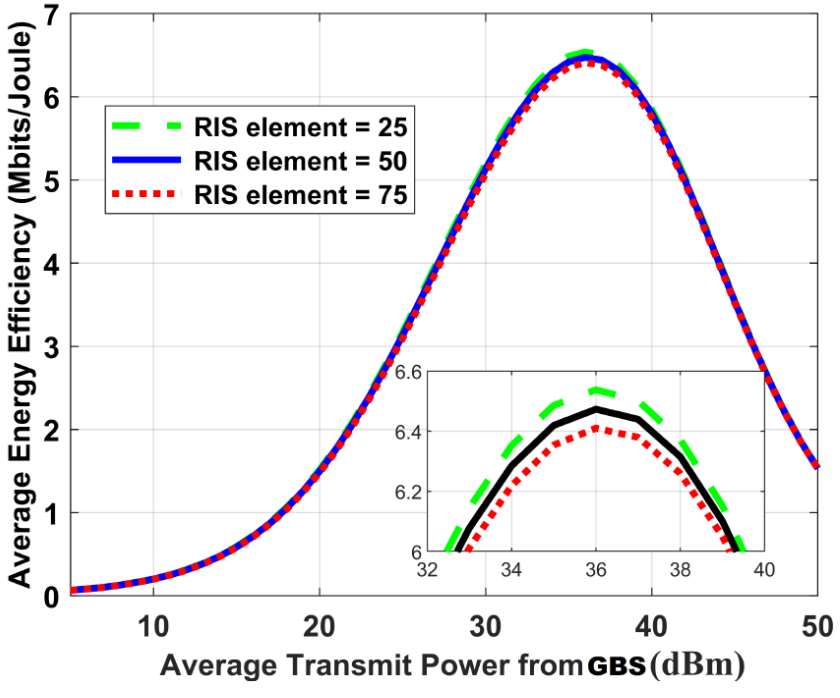

Figures 9 to 12 show the applicability of various channel coding and signal detection techniques to quantify BER for different GUs. With careful analysis of the BER curves shown in Figures 9 to 12, with the combination of Zero Forcing (ZF), Minimum Mean Square Error (MMSE), Cholesky decomposition-based Zero Forcing (ZF) and Lattice reduction-based MMSE (LR-MMSE) signal detection techniques, it is evident that RA channel coding outperforms LDPC channel coding in the simulation. It is also clear that when the LR-MMSE signal detection technique is used, the simulation system has superior BER performance compared to all other possible combinations.

Observing the simulation results of GU 1 in Figure 9, the approximate BER value of MMSE reduces from 0.0018 to 0.0011 in the LR-MMSE signal detection technique, and the BER value changes from around 31.86 to 0.10% for an ordinary SNR value of 6 dB. In this scenario, the system employing RA channel coding with ZF signal detection achieves a 25.03 dB enhancement over LDPC channel coding with LR-MMSE signal detection under 16-QAM higher-order digital modulation.

Figure 9 BER performance utilising various channel coding and signal detection techniques for GU 1 (see online version for colours)

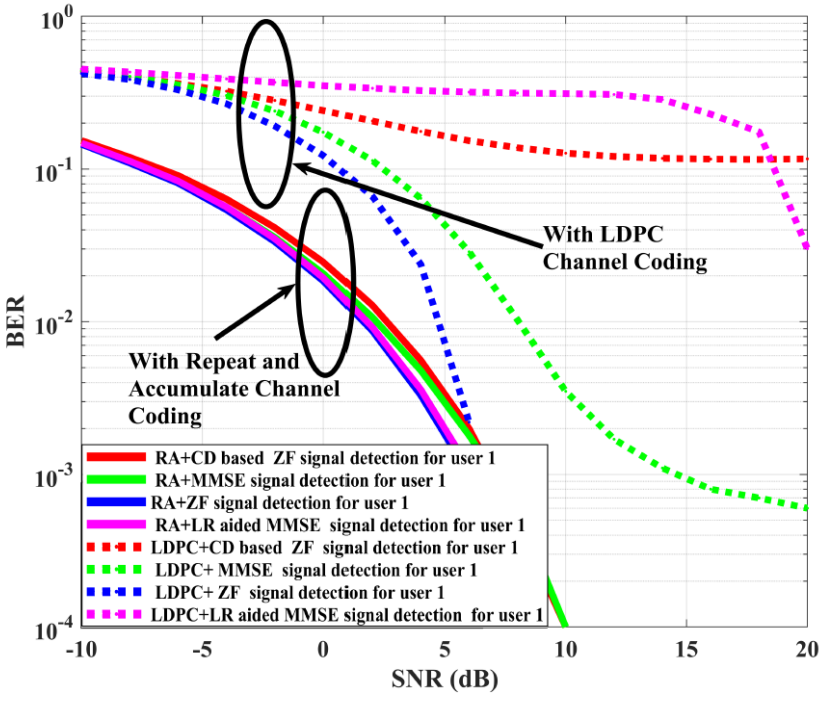

With such a similar assessment of the SNR value for GU 2 in Figure 10, the approximate BER value of MMSE reduces from 0.0061 to 0.0023 in the LR-MMSE signal detection technique and the BER values are found to vary from approximately 31.56 to 0.07%. With these predicted values under 16-QAM, the system using RA channel coding with Cholesky decomposition-based Zero Forcing (ZF) represents an improvement of 16.54 dB over LDPC channel coding with MMSE signal detection approach.

In case of GU 3, in Figure 11, the approximate BER value of MMSE reduces from 0.018 to 0.0017 in LR-MMSE signal detection technique and the BER value varies from approximately 32.13 to 0.14%. Using RA channel coding employing LR-MMSE signal detection technique as compared with LDPC channel coding employing LR-MMSE signal detection technique, a system enhancement of 22.63 dB is attained for the 16-QAM digital modulation case specifically investigated.

Figure 10 BER performance utilising different signal detection and channel coding techniques for GU 2 (see online version for colours)

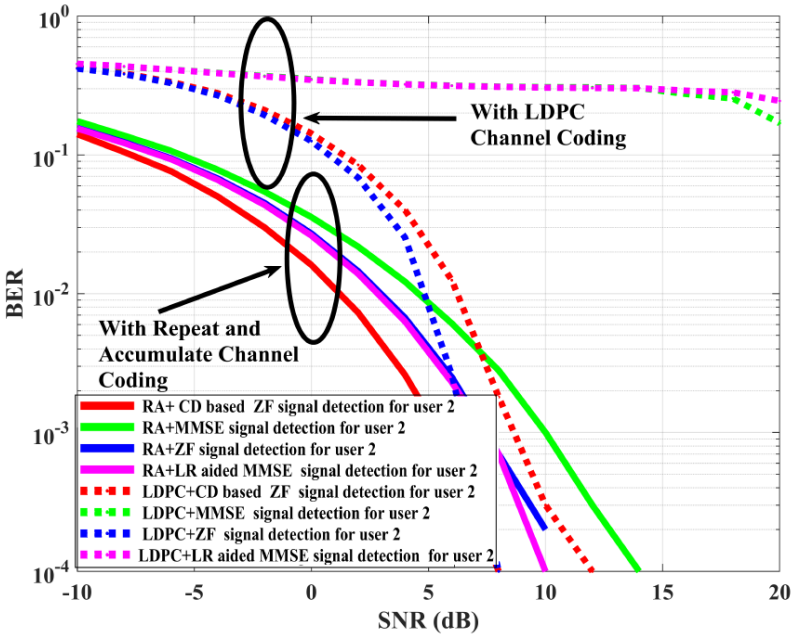

Figure 11 BER performance utilising various channel coding and signal detection techniques for GU 3 (see online version for colours)

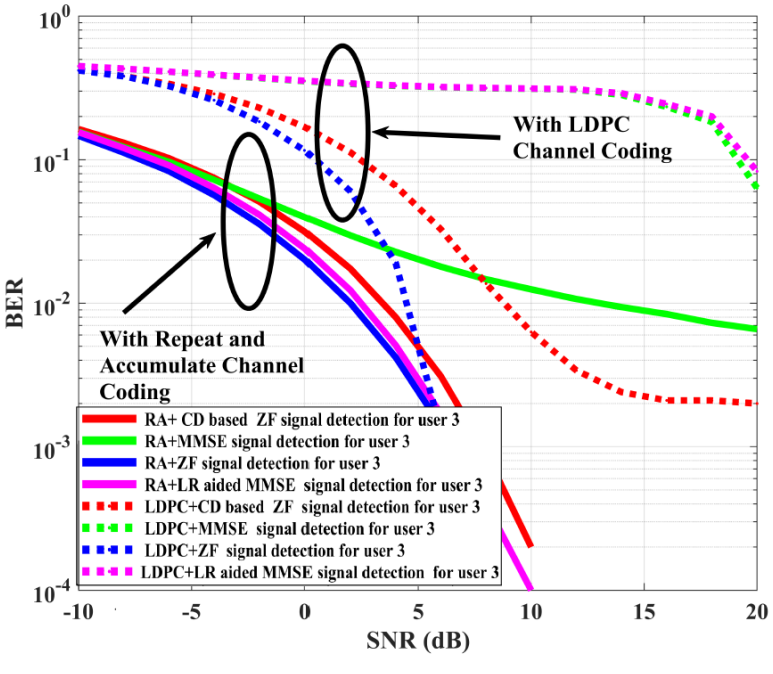

From Figure 12 for GU 4, it is observable that the predicted BER value of MMSE reduces from 0.0443 to 0.0128 in LR-MMSE signal detection technique and the BER values are found to vary from approximately 32.18 to 0.26% for an ordinary SNR value of 6 dB. Figure 11 also shows that the estimated BERs for RA channel coding with ZF signal detection and LDPC channel coding with LR-MMSE signal detection under 16-QAM are 0.0026 and 0.3218, respectively, for RA channel coding with ZF signal detection and LDPC channel coding with LR-MMSE signal detection. In this instance, the predicted parameters are clearly pointing to a systematic improvement of 23.03 dB.

Figure 12 BER performance utilising different signal detection and channel coding techniques for GU 4 (see online version for colours)

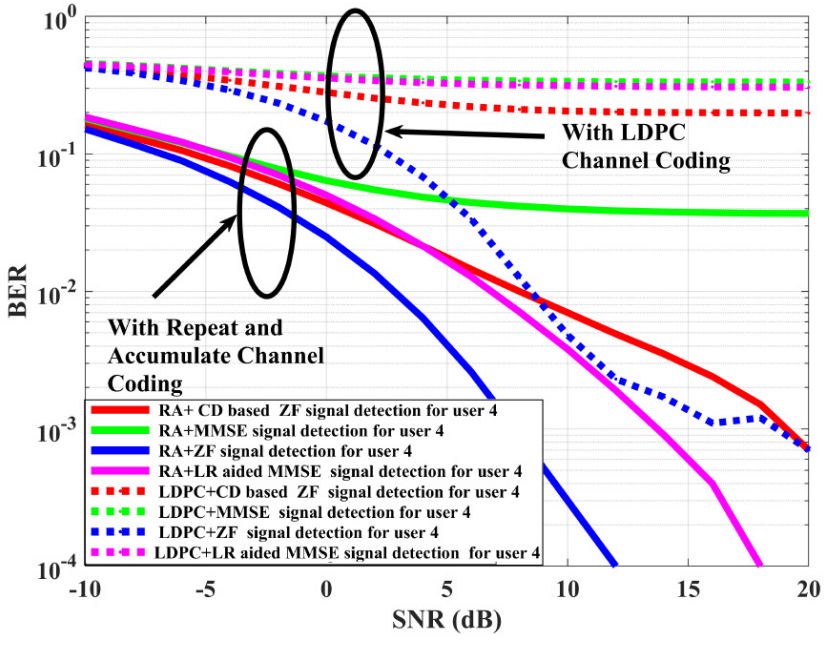

4 Conclusion

In this paper, a design methodology for a transceiver for a UAV-mounted RIS-based downlink 6G compatible multi-user NOW system is presented. In the proposed system, GUs are receiving dominant signals in transmission from the GBS via RIS. In the case of direct transmission from the GBS to the GUs, the presence of skyscrapers in urban areas has a blocking effect. The simulation results demonstrate the efficiency of the proposed system in terms of enhanced BER performance with higher-order digital modulation. According to the findings, the deployment of RA channel coding with CD-based ZF signal detection technique or LR-MMSE delivered superior performance. In the future, we plan to extend the proposed model to accommodate imperfect channel state information (Li et al., 2024).

References

Abualhayja'a, M., Centeno, A., Mohjazi, L., Butt, M.M., Sehier, P., Abbasi, Q.H. and Imran, M.A. (2021) 'Performance of reconfigurable intelligent surfaces vs. relaying for UAV-assisted communications', *Proceedings of the IEEE USNC-URSI Radio Science Meeting (Joint with AP-S Symposium)*, IEEE, pp.58–59.

Al-Hourani, A., Kandeepan, S. and Lardner, S. (2014) 'Optimal lap altitude for maximum coverage', *IEEE Wireless Communications Letters*, Vol. 3, No. 6, pp.569–572.

Asmoro, K. and Shin, S.Y. (2022) 'Ris grouping based index modulation for 6g telecommunications', *IEEE Wireless Communications Letters*, Vol. 11, No. 11, pp.2410–2414.

Bai, L. and Choi, J. (2012) *Low Complexity MIMO Detection*, Springer Science & Business Media.

Chen, Z., Chen, G., Tang, J., Zhang, S., So, D.K.C., Dobre, O.A., Wong, K.K. and Chambers, J. (2022) 'Reconfigurable intelligent surface-assisted b5g/6g wireless communications: challenges, solution and future opportunities', *IEEE Communications Magazine*, Vol. 61, No. 1, pp.16–22.

Cheng, N., Wu, S., Wang, X., Yin, Z., Li, C., Chen, W. and Chen, F. (2023) 'Ai for UAV-assisted IoT applications: A comprehensive review', *IEEE Internet of Things Journal*, Vol. 10, No. 16, pp.14438–14461.

Cui, M., Wu, Z., Lu, Y., Wei, X. and Dai, L. (2022) 'Near-field communications for 6g: fundamentals, challenges, potentials, and future directions', *IEEE Communications Magazine*, pp.1–7.

ETSI (2018) *Technical Specification on 5g nr; Physical Layer; General Description*, Technical Report, 3GPP TS 38.201 version 15.0.0 Release 15.

Faruk, M.O., Sadique, J.J., Cumanan, K. and Ullah, S.E. (2023) 'Orthogonal variable spreading factor encoded unmanned aerial vehicle-assisted nonorthogonal multiple access system with hybrid physical layer security', *ETRI Journal*, Vol. 45, No. 2, pp.213–225.

Gangarajaiah, R., Prabhu, H., Edfors, O. and Liu, L. (2017) 'A cholesky decomposition based massive MIMO uplink detector with adaptive interpolation', *Proceedings of the IEEE International Symposium on Circuits and Systems (ISCAS)*, IEEE, pp.1–4.

Hassouna, S., Rains, J., Kazim, J.R., Rehman, M.U., Imran, M. and Abbasi, Q.H. (2022) 'Discrete phase shifts for intelligent reflecting surfaces in OFDM communications', *Proceedings of the International Workshop on Antenna Technology (iWAT)*, IEEE, pp.128–131.

Huang, C., Zappone, A., Alexandropoulos, G.C., Debbah, M. and Yuen, C. (2019) 'Reconfigurable intelligent surfaces for energy efficiency in wireless communication', *IEEE Transactions on Wireless Communications*, Vol. 18, No. 8, pp.4157–4170.

Jiang, Y. (2010) *A Practical Guide to Error-Control Coding using MATLAB*, Artech House.

Li, X., Zhang, M., Chen, H., Han, C., Li, L., Do, D-T., Mumtaz, S. and Nallanathan, A. (2024) 'Uav-enabled multi-pair massive MIMO-NOMA relay systems with low-resolution ADCS/DACS', *IEEE Transactions on Vehicular Technology*, Vol. 73, No. 2, pp.2171–2186.

Liu, J., Liu, W., Hou, X., Kishiyama, Y., Chen, L. and Asai, T. (2020) 'Non-orthogonal waveform (now) for 5g evolution and 6g', *Proceedings of the IEEE 31st Annual International Symposium on Personal, Indoor and Mobile Radio Communications*, IEEE, pp.1–6.

Rappaport, T.S. (2002) 'Wireless communications–principles and practice, (the book end)', *Microwave Journal*, Vol. 45, No. 12, pp.128–129.

Saad, W., Bennis, M., Mozaffari, M. and Lin, X. (2020) *Wireless Communications and Networking for Unmanned Aerial Vehicle*, Cambridge University Press.

Sabuj, S.R., Ahmed, S. and Jo, H-S. (2023) 'Multiple CUAV-enabled MMTC and URLLC services: review of energy efficiency and latency performance', *IEEE Transactions on Green Communications and Networking*, Vol. 7, No. 3, pp.1369–1382.

Sabuj, S.R., Asiedu, D.K.P., Lee, K-J. and Jo, H-S. (2022) 'Delay optimization in mobile edge computing: cognitive UAV-assisted EMBB and MMTC services', *IEEE Transactions on Cognitive Communications and Networking*, Vol. 8, No. 2, pp.1019–1033.

Sadique, J.J., Sabuj, S.R., Ullah, S.E., Hossain, M.A., Raad, R., Islam, M.R., Kouzani, A.Z. and Mahmud, M.A.P. (2021) 'Analytical framework of CP-free multiuser OFDM system for coordinated multi-point at mmwave', *Applied Sciences*, Vol. 11, No. 16. Doi: 10.3390/app11167605.

Sadique, J.J., Sabuj, S.R., Ullah, S.E., Joarder, S.K. and Hamamura, M. (2022) 'Uav-aided transceiver design for secure downlink OW-DFTS-OFDM system: a multi-user mmwave application', *IEEE Access*, Vol. 10, pp.34577–34590.

Singh, S.K., Agrawal, K., Singh, K., Li, C-P. and Ding, Z. (2022) 'A NOMA-enabled hybrid RIS-UAV-aided full-duplex communication system', *Proceedings of the Joint European Conference on Networks and Communications & 6G Summit (EuCNC/6G Summit)*, IEEE, pp.529–534.

Tanangsanakool, S., Reangsuntea, P., Mori, K. and Boonsrimuang, P. (2020 'Low complexity equalization method for ZP-OFDM under highly mobile environments', *Proceedings of the 22nd International Conference on Advanced Communication Technology (ICACT)*, IEEE, pp.12–17.

Vitetta, G.A., Taylor, D.P., Colavolpe, G., Pancaldi, F. and Martin, P.A. (2013) *Wireless Communications: Algorithmic Techniques*, John Wiley & Sons.

Wu, J., Fang, S., Li, L. and Yang, Y. (2014) 'Qr decomposition and gram Schmidt orthogonalization based low-complexity multi-user MIMO precoding', *10th International Conference on Wireless Communications, Networking and Mobile Computing*, IET, Beijing.

Xie, X., Rong, B. and Kadoch, M. (2021) *6G Wireless Communications and Mobile Networking*, Bentham Science Publishers.

Yin, Z., Cheng, N., Song, Y., Hui, Y., Li, Y., Luan, T.H. and Yu, S. (2024) 'UAV-assisted secure uplink communications in satellite-supported IoT: secrecy fairness approach', *IEEE Internet of Things Journal*, Vol. 11, No. 4, pp.6904–6915.

Yin, Z., Jia, M., Wang, W., Cheng, N., Lyu, F. and Shen, X. (2019b) 'Max-min secrecy rate for NOMA-based UAV-assisted communications with protected', *Proceedings of the IEEE Global Communications Conference (GLOBECOM)*, IEEE, pp.1–6.

Yin, Z., Jia, M., Wang, W., Cheng, N., Lyu, F., Guo, Q. and Shen, X. (2019a) 'Secrecy rate analysis of satellite communications with frequency domain NOMA', *IEEE Transactions on Vehicular Technology*, Vol. 68, No. 12, pp.11847–11858.

You, L., Xiong, J., Ng, D.W.K., Yuen, C., Wang, W. and Gao, X. (2020) 'Energy efficiency and spectral efficiency tradeoff in RIS-aided multiuser MIMO uplink transmission', *IEEE Transactions on Signal Processing*, Vol. 69, pp.1407–1421.

Zaidi, A.A., Baldemair, R., Molés-Cases, V., He, N., Werner, K. and Cedergren, A. (2018) 'OFDM numerology design for 5g new radio to support IoT, EMBB, and MBSFN', *IEEE Communications Standards Magazine*, Vol. 2, No. 2, pp.78–83.

Zhai, Z., Dai, X., Duo, B., Wang, X. and Yuan, X. (2022) 'Energy-efficient UAV-mounted RIS assisted mobile edge computing', *arXiv preprint arXiv:2203.12799*.

Zhang, H., Di, B., Song, L. and Han, Z. (2021a) *Reconfigurable Intelligent Surface-Empowered 6G*, Springer.

Zhang, Z., Zhang, C., Jiang, C., Jia, F., Ge, J. and Gong, F. (2021b) 'Improving physical layer security for reconfigurable intelligent surface aided NOMA 6g networks', *IEEE Transactions on Vehicular Technology*, Vol. 70, No. 5, pp.4451–4463.